International Journal of Neural Systems, Vol. 23, No. 2 (2013) 1350005 (10 pages)

DOI: 10.1142/S0129065713500056

# PERCEPTUAL SUPPRESSION REVEALED BY ADAPTIVE MULTI-SCALE ENTROPY ANALYSIS OF LOCAL FIELD POTENTIAL IN MONKEY VISUAL CORTEX

MENG HU and HUALOU LIANG*
*School of Biomedical Engineering*
*Science & Health Systems, Drexel University*
*Philadelphia, Pennsylvania 19104, USA*
**hualou.liang@drexel.edu*

Accepted 20 December 2012
Published Online 28 February 2013

Generalized flash suppression (GFS), in which a salient visual stimulus can be rendered invisible despite continuous retinal input, provides a rare opportunity to directly study the neural mechanism of visual perception. Previous work based on linear methods, such as spectral analysis, on local field potential (LFP) during GFS has shown that the LFP power at distinctive frequency bands are differentially modulated by perceptual suppression. Yet, the linear method alone may be insufficient for the full assessment of neural dynamic due to the fundamentally nonlinear nature of neural signals. In this study, we set forth to analyze the LFP data collected from multiple visual areas in V1, V2 and V4 of macaque monkeys while performing the GFS task using a nonlinear method — adaptive multi-scale entropy (AME) — to reveal the neural dynamic of perceptual suppression. In addition, we propose a new cross-entropy measure at multiple scales, namely adaptive multi-scale cross-entropy (AMCE), to assess the nonlinear functional connectivity between two cortical areas. We show that: (1) multi-scale entropy exhibits percept-related changes in all three areas, with higher entropy observed during perceptual suppression; (2) the magnitude of the perception-related entropy changes increases systematically over successive hierarchical stages (i.e. from lower areas V1 to V2, up to higher area V4); and (3) cross-entropy between any two cortical areas reveals higher degree of asynchrony or dissimilarity during perceptual suppression, indicating a decreased functional connectivity between cortical areas. These results, taken together, suggest that perceptual suppression is related to a reduced functional connectivity and increased uncertainty of neural responses, and the modulation of perceptual suppression is more effective at higher visual cortical areas. AME is demonstrated to be a useful technique in revealing the underlying dynamic of nonlinear/nonstationary neural signal.

*Keywords*: Perceptual suppression; local field potential; adaptive multi-scale entropy; nonlinear functional connectivity.

## 1. Introduction

It has been well accepted that visual perception is not a simple projection of the external world, but instead involves internal processes in the brain that organize and interpret sensory inputs.[1] To study the neural basis of visual perception, it is important to design an experimental paradigm in which percepts are dissociated from the visual inputs. Generalized flash suppression (GFS) is such an experimental paradigm, where a salient visual stimulus can be rendered invisible despite continuous retinal input, thus it dissociates the perception from the physical stimulus, providing a rare opportunity for directly studying the neural mechanisms of visual perception.[2]

Much evidence has shown that the local field potential (LFP) is modulated by various cognitive

processes and may therefore reflect neural processing at a population level.[3–5] As such, the study of how LFP is related to perceptual reports during physically identical but perceptually different conditions may shed new lights on the mechanism of neural information processing and the neural basis of visual perception. A previous study using linear analysis methods has shown that the LFP power at different frequency bands are differentially modulated by perceptual suppression within the GFS paradigm.[6] Yet, given the fundamentally nonlinear nature of neural dynamic, linear methods alone may be insufficient to provide a full assessment of cortical activities.[7,8]

In this study, we set forth to analyze the LFP data collected from multiple visual cortices (V1, V2 and V4) of monkeys while performing a GFS task using nonlinear methods, i.e. the recently developed adaptive multi-scale entropy (AME)[9] and its cross-entropy extension for measuring multi-scale nonlinear connectivity, namely adaptive multi-scale cross-entropy (AMCE). The goal of this study herein is twofold: (1) the use of AME measure of LFP within each visual cortical area to characterize and compare the percept-related changes and (2) the use of AMCE measure between different visual cortical areas to characterize the percept-related functional connectivity changes. As such, we first employ the AME to measure the regularity of the LFP data under different perceptual conditions (Visible versus Invisible) over the multiple temporal scales. The AME is a multi-scale analysis method, in which the scales are adaptively derived directly from the data by virtue of multivariate empirical mode decomposition (MEMD),[10] which is fully data-driven, well suited for the analysis of nonlinear/nonstationary neural data. Depending on the consecutive removal of low-frequency or high-frequency components, the AME can be estimated at either coarse-to-fine (preserving high-frequency oscillations by progressively removal of low-frequency components) or fine-to-coarse scales (preserving low-frequency oscillations by progressively removal of high-frequency components), over which the sample entropy[11] is performed. Second, by virtue of cross-sample entropy[11] that measures the degree of the asynchrony between two time series, we extend the AME algorithm to the AMCE to assess the nonlinear functional connectivity of neural recordings from different visual cortical areas over the multiple scales of LFP data.

The paper is organized as follows. In Sec. 2, we first briefly describe the experimental details and electrophysiological data used in this work, then recapitulate sample entropy, cross-sample entropy and MEMD upon which our AME and AMCE methods are proposed. In Sec. 3, we apply our approach to LFP from multiple cortical areas (V1, V2 and V4) of two monkeys while performing GFS tasks to examine (1) how perceptual alternation modulates neural activity over different cortical areas; and (2) how functional connectivity between cortical areas reflects different perceptual conditions. Section 4 concludes with discussion.

## 2. Materials and Methods

### 2.1. *Experimental task and electrophysiological recordings*

The GFS task is a visual illusion task where a salient visual stimulus (target) can be rendered invisible despite continuous retinal input.[2] It dissociates the percepts from visual inputs, thus providing a rare opportunity to study neural mechanisms directly related to perception. Here, we recapitulate the GFS task and neural data used in this report. For a more detailed description, please see the Ref. 6.

Monkeys were trained, initially with unambiguous stimuli, to pull a lever whenever a target was visible, and to release lever when the target disappeared. Once the monkeys learned to respond correctly with unambiguous stimuli, real GFS stimulation trials were introduced, which were interleaved with unambiguous, catch trials. Throughout the experiment, catch trials were used to control the monkey's correct behavior, which was validated by psychophysical testing.

In the task, a typical trial started with a warning tone followed by the onset of a fixation spot, which was a small yellow spot (0.15°) in the middle of the screen. As soon as a monkey gained fixation for about 300 ms, the target stimulus indicated by a red disk with a size of 1.0° was presented. The target position was selected based on receptive field properties mapped in each session for at least one of the recording sites. At 1400 ms after the target onset, small random-moving dots appeared as the surroundings. With the immediate presence of the surroundings, the red disk could be rendered subjective invisible, though it still stayed physically. Monkeys were

required to maintain fixation throughout the whole trial and to hold a lever as long as the target was visible. If the target became invisible via perceptual suppression, the monkeys released the lever and had to maintain fixation for an additional 800 ms to receive a juice reward. Therefore, based on the responses of the animal, the trial was classified as either "Visible" or "Invisible". Note that the stimuli sequences in these two conditions were physically identical.

Multi-electrode recordings were simultaneously collected from multiple cortical areas V1, V2 and V4 while monkeys performed the GFS task. The LFP data were obtained by band-pass filtering the full bandwidth signal between 1 and 500 Hz, and then resampled at 1 kHz.[6] Data reported in the present study were from two monkeys: one was simultaneously collected from V1 (1 electrode), V2 (4 electrodes) and V4 (4 electrodes) of 59 trials, another was collected simultaneously from V1 (2 electrodes) and V2 (1 electrode) of 65 trials. One-second-long LFP after surrounding onset was used in the analysis.

### 2.2. *Sample entropy and cross-sample entropy*

Both sample entropy and cross-sample entropy[11] are commonly used nonlinear measures. The former is designed to measure the irregularity/randomness of time series, whereas the latter is intended to reflect the degree of asynchrony between two time series.

Among the existing entropy methods, sample entropy is thought of as a robust, powerful nonlinear measure due to its insensitivity to data length and immunity to noise.[12] In order to compute sample entropy, a time series $I = \{i(1), i(2), \ldots, i(N)\}$ is first embedded in a $m$-dimensional space, in which the $m$-dimensional vectors of the time series are constructed as $x_m(k) = (i(k), i(k+1), \ldots, i(k+m-1))$, $k = 1 \sim N-m+1$. In the embedded space, the match of any two vectors is defined as their distance lower than the tolerance $r$. The distance between two vectors refers to the maximum difference between their corresponding scalar components. $B^m(r)$ is defined as the probability that two vectors match within a tolerance $r$ in the $m$-dimensional space, where self-matches are excluded. Similarly, $A^m(r)$ is defined in the $m+1$-dimensional space. Sample entropy is then defined as the negative natural logarithm of the conditional probability that two sequences similar for $m$ points remain similar at the next $m+1$ point in the data set within a tolerance $r$, which is calculated as:

$$\mathrm{SampEn}(I, m, r) = -\ln\left(\frac{A^m(r)}{B^m(r)}\right)$$

Cross-sample entropy[11] that measures the degree of asynchrony between two related time series is very similar to sample entropy in design, differing only in that it compares sequences from one time series with those from another. In order to compute cross-sample entropy between two time series $I = \{i(1), i(2), \ldots, i(N)\}$ and $U = \{u(1), u(2), \ldots, u(N)\}$, both time series are first embedded in the $m$-dimensional space, where the $m$-dimensional vectors of two time series are constructed as $x_m(k) = (i(k), i(k+1), \ldots, i(k+m-1))$ and $y_m(p) = (u(p), u(p+1), \ldots, u(p+m-1))$, $k, p = 1 \sim N-m+1$, respectively. $B^m(r)(U \parallel I)$ is the probability that the sequences of time series $I$ match the sequences of time series $U$ within $r$ for $m$ points. Similarly, $A^m(r)(U \parallel I)$ is defined for an embedded dimension of $m+1$. The cross-sample entropy is then calculated as:

$$\begin{aligned}&\mathrm{cross\_SampEn}(I, U, m, r)\\ &\quad = -\ln\left(\frac{A^m(r)(U \parallel I)}{B^m(r)(U \parallel I)}\right)\end{aligned}$$

The selection of parameters for $m$ and $r$ is critical in the calculation of sample entropy and cross-sample entropy. In this study, $m$ and $r$ were chosen as 2 and 0.15 for minimizing the standard error of entropy estimation, in accordance with the Ref. 13. Although sample entropy and cross-sample entropy have been successfully applied to the analysis of physiologic signals,[14,15] both are single-scale measures which may fail to account for multiple scales inherent in such time series. In the present study, we adaptively extract the scales of data by virtue of MEMD.[10]

### 2.3. *Multivariate empirical mode decomposition*

MEMD is a multi-variate extension of empirical mode decomposition (EMD). The EMD[16] acts as a fully adaptive data-driven method which decomposes a time series into a finite set of scale-dependent intrinsic mode functions (IMFs), which represent its inherent oscillatory modes. Specifically, for a time

series $x(t)$, all the local extrema are first identified, and then two envelops $e_{\min}(t)$ and $e_{\max}(t)$ are obtained by interpolating between local maxima (respectively minima) to compute the local mean $m(t) = (e_{\min}(t)+e_{\max}(t))/2$. The detail $c(t) = x(t)-m(t)$ is finally iterated until it becomes an IMF (the symmetric envelops and the same numbers of zero-crossing and local extrema, differing at most by one). The residue by removing IMFs from raw signal is subject to the above procedure for the next IMF until the monotonic residue is left. Hence, a time series $x(t)$ can be expressed as: $x(t) = \sum_{j=1}^{N} C_j(t) + r(t)$, where $C_j(t)$, $j = 1, \ldots, N$ are the IMFs, and $r(t)$ is the residue.

Although the EMD has become an established tool for the analysis of the univariate time series, the mode-misalignment and the mode-mixing problems limit its further application on the multivariate time series. MEMD,[10] as a multivariate extension of EMD, renders the IMFs aligned, and also entails an attractive property similar to EMD having a filter bank structure for a multivariate white noise.[17] An important step in the MEMD method is the calculation of local mean, as the concept of local extrema is not well defined for multivariate signals. To deal with this problem, MEMD projects the multivariate signal along different directions to generate the multiple multi-dimensional envelops; these envelops are then averaged to obtain the local mean. For an $n$-variable signal, the MEMD algorithm is briefly summarized as follows:

(i) Construct the suitable point set (e.g. the Hammersley sequence) for sampling on an $(n-1)$-sphere;
(ii) Compute a projection $\{p^{\theta_k}(t)\}_{t=1}^{T}$ of the multivariate input data $\{v(t)\}_{t=1}^{T}$ along a direction vector $x^{\theta_k}$ for all $k$ giving $\{p^{\theta_k}(t)\}_{k=1}^{K}$;
(iii) Locate the timepoints $t_i^{\theta_k}$ according to maxima of the set of projected signal $\{p^{\theta_k}(t)\}_{k=1}^{K}$;
(iv) Interpolate $[t_i^{\theta_k}, v(t_i^{\theta_k})]$ to acquire multivariate envelope curves $\{e^{\theta_k}(t)\}_{k=1}^{K}$;
(v) Calculate the mean $m(t)$ of the envelop curves for a set of $K$ direction vectors, $m(t) = (1/K)\sum_{k=1}^{K} e^{\theta_k}(t)$;
(vi) Iterate on the detail $c(t) = x(t) - m(t)$ until it becomes an IMF. The above procedure is applied to the residue $r(t) = x(t) - c(t)$.

### 2.4. *AME and AMCE*

As a multi-scale entropy analysis method, AME[9] was recently developed to calculate the sample entropy over multiple scales of data extracted by MEMD. As described above, MEMD is a fully data-driven method, which adaptively decomposes multivariate data into a finite set of IMFs aligned in both number and frequency scale, thus is applicable to the analysis of multivariate data.

Nonetheless, direct application of MEMD to neural data is usually problematic. First, neural data are often collected over certain time period from multiple channels across many trials, which can be represented as a three-dimensional matrix, i.e. TimePoints × Channels × Trials. The MEMD method cannot directly process this kind of high-dimension data. Second, neural recordings are usually collected over many trials spanning from days to months, or even years, so that the dynamic ranges of signals are likely to be of high degree of variability. Since the MEMD deals with multivariate data by projecting them in the multi-dimensional spaces, the high degree of variability has significant detrimental bias upon the final decomposition of MEMD. Therefore, two important preprocessing steps[18] should be taken before applying the MEMD to the neural data. First, the high-dimensional neural data (e.g. TimePoints × Channels × Trials) is first reshaped into such a two-dimensional time series as TimePoints × [Channels × Trials] before submitted for the MEMD analysis. It is an important step to make sure that all the IMFs be aligned not only across channels, but also across trials. Second, in order to reduce the variability among neural recordings, individual time series in the reshaped matrix is normalized against their temporal standard deviation before the MEMD is applied. After the MEMD decomposition, those extracted standard deviations are then restored to the corresponding IMFs.

After performing the MEMD on our neural data to obtain the aligned IMFs (Say, $N$ IMFs), the scales of each time series can be determined by consecutively removing its either high-frequency or low-frequency IMFs from the raw time series, which results in two scale-evolving decompositions, namely the fine-to-coarse ($S_{f2c}^{k} = \sum_{i=k}^{N} \text{IMF}_i, k \leq N$) and the coarse-to-fine ($S_{c2f}^{k} = \sum_{i=1}^{N+1-k} \text{IMF}_i, k \leq N$). Both decompositions can each be used separately or

used in tandem to reveal underlying dynamic of complex neural data. Hence, the AME is readily obtained by calculating the sample entropy over these adaptive scales. For the calculation of AMCE, after extracting scales of data, the cross-sample entropy can be applied between two channels at a given scale within each trial. Note that the AMCE here is only calculated between two time series at the same scale of individual trials between different visual cortical areas.

Having obtained the AME (AMCE) at individual scales, we averaged it across trials and channels (between channels) within a cortical area (between areas). A $t$-test was applied at each scale to determine statistical significance of the AME or AMCE.

## 3. Results

In this study, the use of GFS task is a major strength since it allows dissociation between stimuli and perception and thus provides a rare opportunity for directly studying neural underpinnings related to the percepts rather than to the stimulus. Considering the nonlinear nature of neural signal, we focus on the AME analysis of LFP during GFS. Figure 1 shows representative single-trial LFP recordings at three visual cortical areas (V1, V2 and V4) together with their coarse-to-fine and fine-to-coarse decompositions.

First, we apply the AME method to LFP data during GFS to study how perceptual suppression modulates neural activity. For the coarse-to-fine AME (see Fig. 2), we can see that the entropy measures from different cortical areas show similar increasing trend as the scale increases, and the LFP activity in the invisible condition (perceptual suppression), in general, exhibits larger entropy than that in the visible condition over multiple LFP scales. Meanwhile, it is clear to see that higher visual cortical area shows larger discrimination between different perceptual conditions over these scales. Specifically, the entropies of invisible and visible conditions overlap at area V1 [see Fig. 2(a)]. However, at area V2 [see Fig. 2(b)], the invisible condition shows the significantly greater entropy than the visible condition at the 1st–7th scales ($p < 0.05$), where the largest separation occurs at the 6th scale (note that the first scale refers to the raw data). Furthermore, the changes of entropy across these scales in area V4 [see Fig. 2(c)] show even larger separation ($p < 0.01$) between two conditions than observed in area V2, where the largest separation also occurs at the 6th scale.

For the fine-to-coarse AME (see Fig. 3), similar observations are obtained as the coarse-to-fine AME except that the entropy displays the decreased trend as the scale increases. Specifically, the invisible condition shows the higher entropy than the visible condition over several scales and the higher visual cortical area retains the more discriminative information for distinguishing different conditions. The AME results at both the coarse-to-fine and the fine-to-coarse scales together suggest that perceptual suppression may be related to the more random neural information processing, and the effect of perceptual suppression is more pronounced at higher visual cortical area.

Second, we apply the AMCE to the LFP time series between different visual cortical areas (i.e.

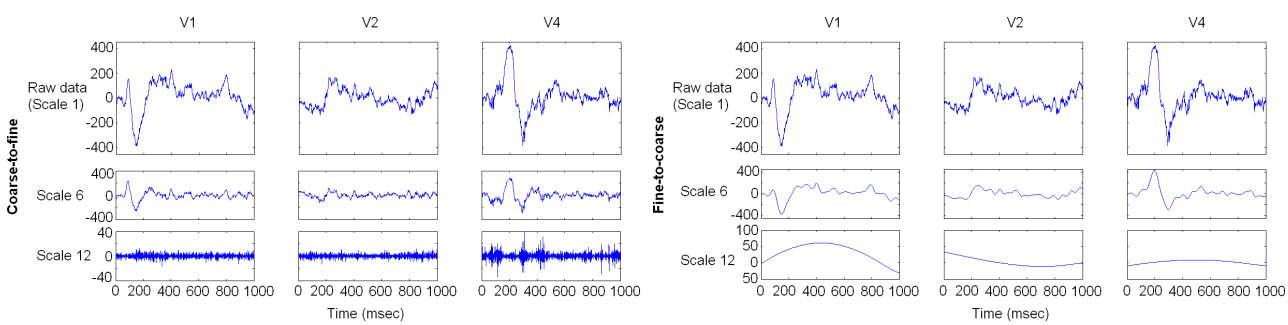


Fig. 1. Representative single-trial LFP recordings at three visual cortical areas (V1, V2 and V4) are represented along the coarse-to-fine (left) and fine-to-coarse (right) decompositions. In this study, the LFP time series analyzed is one-second-long after surrounding onset, which is decomposed into 12 IMFs, thus yielding 12 scales for each decomposition. Note that data only at the first (raw data), the sixth and the last scales are shown for illustration.

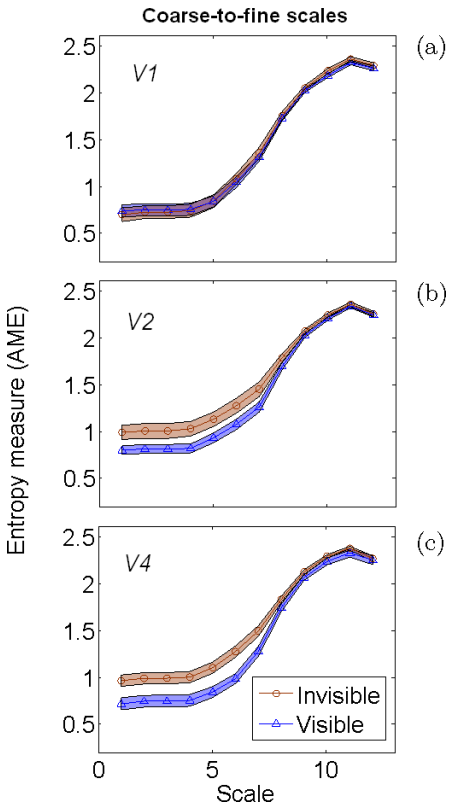


Fig. 2. (Color online). Coarse-to-fine AME results for two perceptual conditions, Invisible (red circles) versus Visible (blue triangles) at three visual cortical areas: V1 (a), V2 (b) and V4 (c). Thick lines with shaded traces depict the mean and the standard error of mean. The leftmost red circle and blue triangle are the entropy of the raw data.

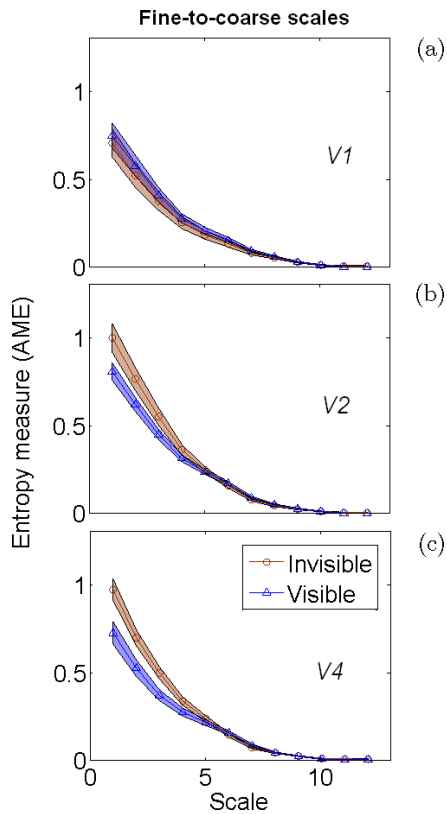


Fig. 3. (Color online). Fine-to-coarse AME results for two perceptual conditions, Invisible (red circles) versus Visible (blue triangles) at three visual cortical areas: V1 (a), V2 (b) and V4 (c). Thick lines with shaded traces depict the mean and the standard error of mean. The leftmost red circle and blue triangle are the entropy of the raw data.

V1–V2, V1–V4 and V2–V4) to investigate how perceptual suppression affects functional connectivity between cortical areas. The results of the coarse-to-fine AMCE (see Fig. 4) clearly show that the invisible condition exhibits weaker functional connectivity (the larger asynchrony measure) between areas than the visible condition for all the pairwise areas, V1–V2 [see Fig. 4(a)], V1–V4 [see Fig. 4(b)] and V2–V4 [see Fig. 4(c)], over the 1st–the 7th scales with the largest separations occurring at the 6th scale. Among all these pairwise measures, the entropy between V1–V2 ($p < 0.05$) shows relatively less discriminative information between two perceptual conditions than other two area-pairs associated to area V4 ($p < 0.01$), which further confirms our finding that the modulation of perceptual suppression is more effective at the higher visual cortical area.

For the fine-to-coarse AMCE (see Fig. 5), the invisible condition also shows weaker connectivity between different areas than the visible condition at multiple scales. The cross-entropies for V1–V4 [see Fig. 5(b)] and for V2–V4 [see Fig. 5(c)] show larger separation between different conditions than that for V1–V2 [see Fig. 5(a)]. The AMCE results at both the coarse-to-fine and the fine-to-coarse scales suggest that perceptual suppression is likely related to the reduced functional connectivity between visual cortical areas and the effect of perceptual suppression is again more significant at the higher visual cortical area.

In comparison of the coarse-to-fine to the fine-to-coarse AMEs (Figs. 2 and 3, respectively), and similarly AMCEs (Figs. 4 and 5, respectively), we can see that the coarse-to-fine AME (preserving

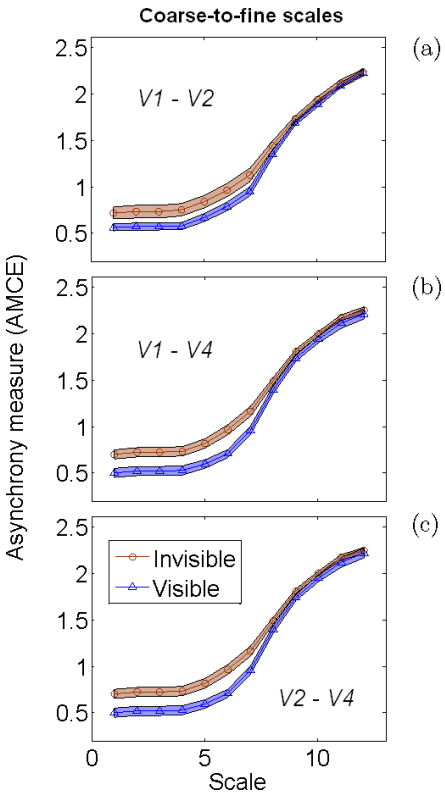


Fig. 4. (Color online). Coarse-to-fine AMCE results for two perceptual conditions, Invisible (red circles) versus Visible (blue triangles) between different areas: V1–V2 (a), V1–V4 (b) and V2–V4 (c). Thick lines with shaded traces depict the mean and the standard error of mean. The leftmost red circle and blue triangle are the cross-entropy of the raw time series.

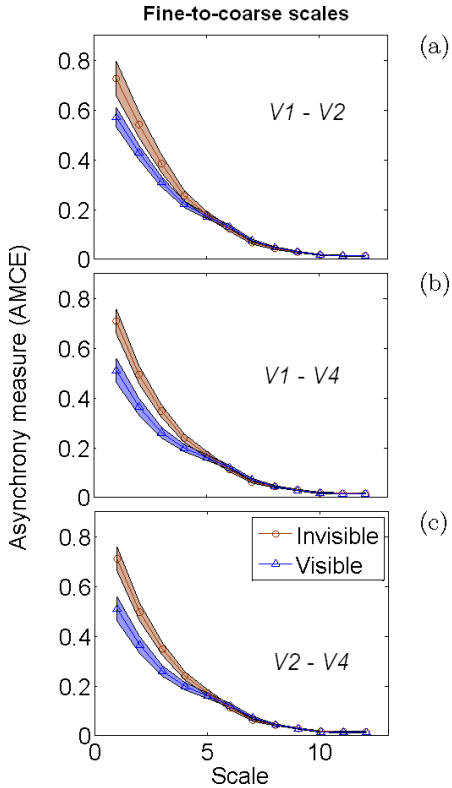


Fig. 5. (Color online). Fine-to-coarse AMCE results for two perceptual conditions, Invisible (red circles) versus Visible (blue triangles) between different area-pairs: V1–V2 (a), V1–V4 (b) and V2–V4 (c). Thick lines with shaded traces depict the mean and the standard error of mean. The leftmost red circle and blue triangle are the cross-entropy of the raw time series.

high-frequency oscillations) exhibits more discriminative information for distinguishing two perceptual conditions than the fine-to-coarse AME (preserving low-frequency oscillations), which indicates that the low-frequency oscillations may not contain as much discriminative information as the high-frequency. The low-frequency oscillations correspond to the evoked potentials, which are presumably the same as the stimuli in the GFS task are identical; this explains why the entropy at the fine-to-coarse scales exhibit less discriminative ability for separating two perceptual conditions.

## 4. Discussion

In this paper, we focus on the nonlinear multi-scale entropy analysis of LFP during GFS task for characterizing the neural dynamic of perceptual suppression. Specifically, considering the multiple scale structure of LFP time series, we first employ the recently developed AME to analyze LFP collected from multiple visual cortical areas (V1, V2 and V4) of monkey while performing GFS task over the multiple adaptive scales of data, for studying the modulation of neural activity by perceptual suppression. We then extend the AME method to AMCE to assess the nonlinear functional connectivity between different visual cortical areas, for investigating how perceptual suppression affects the functional connectivity between visual cortical areas.

Our results show that the invisible condition (perceptual suppression) exhibits larger entropy (or higher uncertainty) and reduced functional connectivity between different cortical areas than the visible condition over multiple LFP scales, and the higher visual cortical area retains more discriminative information between different perceptual conditions.

These results suggest that reduced or even breakdown of functional connectivity decreases the visual stability, thus increased uncertainty, leading up to perceptual suppression. In addition, the modulation of perceptual suppression is more significant at the higher visual cortical areas.

A longstanding debate exists in the literature concerning the neural basis of bistable perception. It is generally thought that bistable perception results from lateral competition between visual representations at some level of the visual pathway, but the nature of the competitive interactions that mediate bistable perception has remained unresolved. Among various theories, the debate has been focused on two competing theories: interocular competition versus pattern competition. Specifically, it is debated whether discrepant percepts rival as a result of low-level interocular competition between monocular channels[19−22] or competition between high-level incompatible pattern representations.[23−25]

Interocular competition theory provides a simple powerful explanation of bistable perception as a competitive process involving reciprocal inhibition between the two eyes. This theory largely underscores automatic, stimulus-driven form of visual competition, it therefore has difficulty to explain the data reported in our analysis as the stimuli in both the visible and the invisible conditions are identical, and thus the low-level features remain intact. Pattern competition theory, on the other hand, seems to provide compelling account of our data. Our entropy analysis revealed much stronger effects in higher visual areas V2 and V4, but no difference of percept-related activity in V1, thus fail to support the predictions of interocular competition. Instead, our findings support the notion that perceptual alternation arises from competition among neurons at much higher levels of the visual pathway. Additionally, our analysis of inter-area functional connectivity provides important insights into the nature of the competitive interactions that mediate bistable perception: reduced or even breakdown of functional connectivity decreases the visual stability, leading to target disappearance (perceptual suppression). Our finding on reduced functional connectivity also generates specific testable predictions that perceptual stability can be disrupted by perturbation of functional connectivity via direct experimental manipulations.

Regarding multi-scale methods, wavelet transform is one of most commonly used methods to perform multi-scale analysis. Wavelet transform is effective in dealing with nonstationary time series, but remains difficult for nonlinear time series.[16] Moreover, wavelet analysis depends on proper choice of the mother wavelet, which is arbitrary and may not be optimal for time series under scrutiny. The EMD and its extensions, on the other hand, is a fully data-driven method without these restrictions.

Our approach benefits from the ability of data-driven EMD method to adaptively decompose nonlinear and nonstationary time series into a number of amplitude or frequency modulated components without any *a priori* assumptions about the data. The EMD method has been used for the analysis of field potentials in visual cortex.[26,27] As any neural recordings are inevitably contaminated by noise, the ability to extract task-relevant responses from the data is naturally compromised, particularly in the presence of strong noise. This has been observed in our laboratory with linear methods such as spectral analysis. By comparison, we found that, although individual scales used in our entropy analysis are tantamount to different frequency bands in spectral analysis, our entropy-based measures are more sensitive than spectral analysis in revealing the difference of precept-related activity.[28] We note that the scales derived from multi-scale entropy analysis are radically different from the frequency bands such as alpha, beta etc, which are somewhat arbitrarily predetermined, yet our scales are adaptively determined by data itself. Together, the combined use of entropy analysis and EMD provides a powerful means to measure the regularity of the data across multiple temporal scales, therefore is a useful technique in revealing the underlying dynamic of nonlinear/nonstationary neural signals.

One drawback with the EMD method is that it lacks an analytical definition due to the empirical nature of the method. Entropy-based measures, on the other hand, are deeply rooted in information theory, hence offers solid theoretical basis. Our entropy-based measures are useful techniques for revealing nonlinear effects, which are certainly abundant in the nervous system. We note that linear methods, when applied properly, most often provide at least a good first approximation to the data, and can reveal a great deal of information about

functional relations among neuronal ensembles. Nonlinear techniques should be considered pending a clear demonstration that the already very general and simple linear techniques are incapable of doing the job.

For the analysis of field potential data, we have demonstrated the use of AME within area and cross-entropy between areas. The observed entropy difference between two perceptual conditions can be used for further analysis, e.g. decoding perceptual states.[29] Therefore, a further step could be the use of entropy measures as features for a classifier to directly identify perceptual states from the LFP data.

## Acknowledgments

This work is partially supported by NIH. We thank Dr. Melanie Wilke for providing the data, which were collected at the laboratory of Dr Nikos Logothetis at Max Planck Institute for Biological Cybernetics in Germany.

## References

1. Y. S. Bonneh, A. Cooperman and D. Sagi, Motion-induced blindness in normal observers, *Nature* **411** (2001) 798–801.
2. M. Wilke, N. K. Logothetis and D. A. Leopold, Generalized flash suppression of salient visual target, *Neuron* **39**(6) (2003) 1043–1052.
3. S. L. Bressler and V. Menon, Large-scale brain networks in cognition: Emerging methods and principles, *Trend. Cogn. Sci.* **14** (2010) 277–290.
4. Z. Wang, A. Maier, N. K. Logothetis and H. Liang, Extraction of bistable-percept-related features from local field potential by integration of local regression and common spatial patterns, *IEEE Trans. Biomed. Eng.* **56**(8) (2009) 2095–2103.
5. Z. Wang, N. K. Logothetis and H. Liang, Decoding a bistable percept with integrated time–frequency representation of single-trial local field potential, *J. Neural Eng.* **5** (2008) 433–442.
6. M. Wilke, N. K. Logothetis and D. A. Leopold, Local field potential reflects perceptual suppression in monkey visual cortex, *Proc. Natl. Acad. Sci. USA* **103** (2006) 17507–17512.
7. N. V. Manyakov, N. Chumerin, and M. M. Van Hulle, Multichannel decoding for phase-coded SSVEP Brain-Computer Interface, *Int. J. Neural Syst.* **22**(5) (2012) 1250022.
8. L. B. Good, S. Sabesan, S. T. Marsh, K. S. Tsakalis and L. D. Iasemidis, Control of synchronization of brain dynamics leads to control of epileptic seizures in rodents, *Int. J. Neural Syst.* **19**(3) (2009) 173–196.
9. M. Hu and H. Liang, Adaptive multiscale entropy analysis of multivariate neural data, *IEEE Trans. Biomed. Eng.* **59**(1) (2012) 12–15.
10. N. Rehman and D. P. Mandic, Multivariate empirical mode decomposition, *Proc. R. Soc. A* **466A** (2010) 1291–1302.
11. J. S. Richman and J. R. Moorman, Physiological time-series analysis using approximate entropy and sample entropy, *Am. J. Physiol-Heart. C* **278** (2000) 2039–2049.
12. M. Costa, A. L. Goldberger and C. K. Peng, Multiscale entropy analysis of complex physiologic time series, *Phys. Rev. Lett* **89**(6) (2002) 068102.
13. D. E. Lake, J. S. Richman, M. P. Griffin and J. R. Moorman, Sample entropy analysis of neonatal heart rate variability, *Am. J. Physiol-RegI.* **283** (2002) R789–R797.
14. E. N. Bruce, M. C. Bruce and S. Vennelaganti, Sample entropy tracks changes in electroencephalogram power spectrum with sleep state and aging, *J. Clin. Neurophysiol.* **26**(4) (2009) 257–266.
15. T. Zhang, Z. Yang and J. H. Coote, Cross-sample entropy statistic as a measure of complexity and regularity of renal sympathetic nerve activity in the rat, *Exp. Physiol.* **92**(4) (2007) 659–669.
16. N. E. Huang, Z. Shen, S. R. Long, M. C. Wu, H. H. Shih, Q. Zheng, N. Yen, C. C. Tung and H. H. Liu, The empirical mode decomposition and the Hilbert spectrum for nonlinear and non-stationary time series analysis, *Proc. R. Soc. A* **454A** (1998) 903–993.
17. N. Rehman and D. P. Mandic, Filter bank property of multivariate empirical mode decomposition, *IEEE Trans. Signal. Process* **59**(5) (2011) 2421–2426.
18. M. Hu and H. Liang, Intrinsic mode entropy based on multivariate empirical mode decomposition and its application to neural data analysis, *Cogn. Neurodyn.* **5**(3) (2011) 277–284.
19. R. Blake, D. H. Westendorf and R. Overton, What is suppressed during binocular rivalry? *Perception* **9**(2) (1980) 223–231.
20. R. Blake, A neural theory of binocular rivalry, *Psychol. Rev* **96**(1) (1989) 145–167.
21. A. Polonsky, R. Blake, J. Braun and D. J. Heeger, Neuronal activity in human primary visual cortex correlates with perception during binocular rivalry, *Nat. Neurosci* **3**(11) (2000) 1153–1159.
22. F. Tong and S. A. Engel, Interocular rivalry revealed in the human cortical blind-spot representation, *Nature* **411** (2001) 195–199.
23. D. A. Leopold and N. K. Logothetis, Activity changes in early visual cortex reflect monkeys'percepts during binocular rivalry, *Nature* **379** (1996) 549–553.
24. N. K. Logothetis and J. D. Schall, Neural correlates of subjective visual perception, *Science* **245** (1989) 761–763.

25. D. L. Sheinberg and N. K. Logothetis, The role of temporal cortical areas in perceptual organization, *Proc. Natl. Acad. Sci. USA* **94**(7) (1997) 3408–3413.
26. Z. Mehboob and H. Yin, Information quantification of empirical mode decomposition and applications to field potentials, *Int. J. Neural Syst.* **21**(1) (2011) 49–63.
27. H. Liang, S. L. Bressler, E. A. Buffalo, R. Desimone and P. Fries, Empirical mode decomposition of field potentials from macaque V4 in visual spatial attention, *Biol. Cybern.* **92** (2005) 380–392.
28. H. Zhang. Neural activity during generalized flash suppression in visual cortex, Ph.D. Dissertation Drexel University, USA (2010).
29. N. V. Manyakov and M. M. Van Hulle, Decoding grating orientation from microelectrode array recordings in monkey cortical area V4, *Int. J. Neural. Syst.* **20**(2) (2010) 95–108.